COBEM2015

ABCM Associação Brasileira de Engenharia e Ciências Mecânicas

23rd ABCM International Congress of Mechanical Engineering
December 6-11, 2015, Rio de Janeiro, RJ, Brazil

TWO NUMERICAL MODELINGS OF FREE CONVECTION HEAT TRANSFER USING NANOFLUIDS

Douglas Hector Fontes
Daniel Dall'Onder dos Santos
Elie Luis Martínez Padilla
Enio Pedone Bandarra Filho
Federal University of Uberlândia, Av. João Naves de Ávila 2121, Uberlândia, MG, 38408-100, Brazil
douglashfontes@hotmail.com
dallonder@femec.ufu.br
epadilla@mecanica.ufu.br
bandarra@mecanica.ufu.br

Abstract. *This work presents numerical results of natural convection flows of water-copper nanofluids inside a square enclosure. Two different numerical methods are employed to approximate the mechanical modeling, namely the finite volume and the finite element methods. The studied nanofluid volumetric concentrations range from 0.1 to 1.0%, with the fluid properties obtained employing experimental and theorical correlations. The simulated nanofluid and water flows have a Rayleigh number ranging from 10^3 to 10^5. The results show almost no difference on the Nusselt number profiles between nanofluids and water, although the convection coefficient is increased on the nanofluids when compared to the base fluid due to the increase on the thermal conductivity.*

Keywords: *water–copper nanofluids, natural convection heat transfer, numerical approximation, Galerkin least-squares method*

1. INTRODUCTION

Several types of heat exchangers that do not require fans or pumps apply heat transfer by natural convection, ensuring very low noise levels. A common application of natural convection heat transfer is in electrical and electronic components and in electrical transformers. With miniaturization and the need to increase the operational performance of these types of equipment, it has become necessary to increase the capacity of heat exchangers. However, in many cases it is not possible to enlarge the exchange surfaces of these systems. An alternative is to improve the thermal properties of the heat exchange fluids, e.g., liquids with a dispersion of nanoscale particles.

In the mid-1990s, researchers observed experimentally that the increase in thermal conductivity (a property of great importance in terms of increasing the thermal exchange capability) of nanoparticle liquid suspensions is underestimated by the equation proposed by Maxwell (1873). Thus, interest in using dispersions of nanoparticles has grown rapidly. Masuda *et al.* (1993) found an increase of about 30% in thermal conductivity using a 4.3% volume concentration of alumina particles (Al_2O_3) in water. Choi and Eastman (1995) presented a theoretical study of dispersions of nanometric particles in liquids, showing the potential of dispersions in heat exchangers – the authors were the first to call this type of dispersion a nanofluid.

The evaluation of the convection coefficients on flows governed by natural convection is often conducted in closed cavities with prescribed thermal boundary conditions. Aiming to analyze the heat exchange capability of nanofluids in natural convection, Putra *et al.* (2003) performed experimentally the natural convection of nanofluids of Al_2O_3 and CuO in water, with volume concentrations of 1% and 4% in an enclosure with a surface maintained at a higher temperature, a surface maintained at a lower temperature, and the other surfaces properly insulated. They observed that the use of nanofluids, in comparison with the base fluid, led to a degradation of the convection mechanism, with smaller Nusselt numbers for the same Rayleigh number. Khanafer *et al.* (2003) numerically evaluated nanofluids on natural convection in a two-dimensional cavity employing a model for the thermal conductivity of nanofluids, wherein the increased thermal conductivity of nanofluids is dependent on the thermal dispersion, which is related to the size of the nanoparticle, the volume concentration, and the velocity field. The authors used copper nanoparticles, with volume concentrations up to 25% water. The authors noticed that the increased volume concentration of nanoparticles led to a growth in the energy transport due to the random motion of nanoparticles, which intensified the thermal dispersion and consequently the thermal conductivity of the nanofluids, increasing the fluid thermal exchange capability.

There is no general agreement between the many results for natural convection inside cavities in the literature – e.g. see Aminossadati and Ghasemi (2009) and Abu-Nada *et al.* (2010). In order to investigate the natural convection heat

transfer inside a square enclosure, this paper presents water–copper nanofluid simulations performed using the finite volume method and a multi-field Galerkin least-squares finite element methodology, which have as primal variables the velocity, pressure, extra-stress, and temperature fields. The addition of mesh-dependent terms on the flow-governing equations makes it possible for the formulation to successfully capture the buoyancy effects present in the employed modeling. The thermal boundary conditions employed are assigned temperatures at the sidewalls and insulation at the top and bottom walls – over all walls, the employed velocity boundary condition is $\mathbf{u} = 0$. The thermal conductivity was set based on experimental results (Wang *et al.*, 2006), and the viscosity was estimated by the correlation found at Batchelor (1977). The mechanical model considers the nanofluid as a single-phase fluid, i.e., there is no slip between the nanoparticles and the base fluid. The heat transfer coefficient was obtained for various Rayleigh numbers and for different volume concentrations of copper nanoparticles in the base fluid (0.1%, 0.5%, and 1.0%).

2. THE MECHANICAL MODEL

The problem analyzed in this work consisted of the flow of water-based copper nanofluids in a closed two-dimensional square enclosure of length L_c subjected to free convection due to a temperature difference between two walls. The employed boundary conditions for the numerical simulations are thermal insulation on the top and bottom walls, prescribed temperature on the side walls, and no-slip and impermeability over all the cavity walls ($\mathbf{u} = 0$), as shown in Fig. 1. In order to ease the numerical approximation, some simplifying hypotheses were considered: the nanofluid is a single-phase incompressible Newtonian fluid with constant physical properties; the nanoparticles and the base fluid are instantaneously in thermal equilibrium, the fluid exhibits laminar flow, and the buoyancy force term is modeled with the Boussinesq approximation.

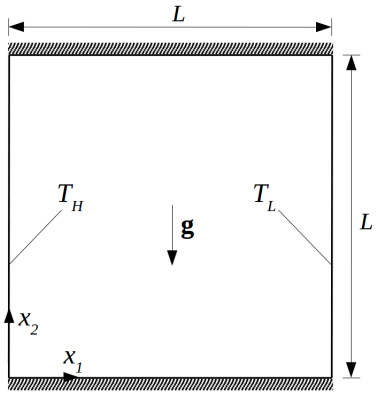

Figure 1. The problem sketch.

The fluid viscosity was evaluated with the correlation proposed by Batchelor (1977) whereas the numerical values of the thermal conductivity were taken from the work of Wang *et al.* (2003). The fluid specific heat is estimated from the first law of thermodynamics and the density from the principle of mass conservation. The physical properties of the nanofluids and the base fluid (water) are shown in Table 1. Therefore, the momentum balance, continuity, and energy equations for the given problem are set as

$$\begin{aligned} &\rho\left(\partial_t \mathbf{u} + (\nabla \mathbf{u})\mathbf{u}\right) = -\nabla p + 2\mu \operatorname{div} \mathbf{D}(\mathbf{u}) + \rho \mathbf{g} \beta (T - T_{ref}) \\ &\operatorname{div} \mathbf{u} = 0 \\ &\rho c_p \left(\partial_t T + (\nabla T)\mathbf{u}\right) = \kappa \nabla^2 T, \end{aligned} \tag{1}$$

where $\mathbf{u}$ is the velocity vector, $\mathbf{D}$ the strain rate tensor, p the hydrostatic pressure, $\mathbf{g}$ the gravity vector, ∂_t the time derivative, T the temperature, and T_{ref} a reference temperature; β is the volumetric thermal expansion coefficient; μ, ρ, c_p, and κ are, respectively, the fluid viscosity, density, specific heat, and thermal conductivity. For the nanofluids, μ is calculated with the correlation proposed by Batchelor (1977), ρ is estimated by Eq. 3 and c_p by Eq. 4; κ is adjusted from experimental data found in the work of Wang *et al.* (2003),

$$\mu = \mu_{bf}\left(1 + 2.5\phi + 6.2\phi^2\right) \tag{2}$$

$$\rho = (1 - \phi)\rho_{bf} + \phi \rho_{np} \tag{3}$$

$$c_p = \frac{(1 - \phi)\, \rho_{bf}\, c_{p_{bf}} + \phi\, \rho_{np}\, c_{p_{np}}}{(1 - \phi)\, \rho_{bf} + \phi\, \rho_{np}} \tag{4}$$

$$\kappa = \kappa_{bf}\left(11.6\phi^2 + 9.6\phi + 1\right), \tag{5}$$

where the subscripts bf, and np indicate, respectively, the fluid base, and nanoparticle properties; ϕ is the dispersed nanoparticles volume concentration in the base fluid.

3. NUMERICAL APPROXIMATION

3.1 The finite volume approximation

Two different numerical methods are employed in this work to approximate the set of equations that represent the mechanical model (Eq. 1). This section describes the approximation by the finite volume method. The computational code has as major features a second-order Runge–Kutta temporal discretization, centered differences interpolation for the variables on each volume face, the use of the fractional steps method for the pressure–velocity coupling, and non-uniform mesh. The obtained algebraic equations are solved by the successive over-relaxation methodology.

In order to validate the numerical code, the Taylor–Green vortices (Taylor and Green (1937)) manufactured solution was used, which has an analytical solution for a two-dimensional domain (Eqs. 6 and 7). Therefore, it is possible to compare the numerical results with the analytical solution, verifying if the flow representative equations are properly implemented. The numerical solution is obtained by imposing the Taylor–Green vortices boundary conditions, where

$$u_1(x_1, x_2) = sin(x_1)cos(x_2)F(t) \tag{6}$$

$$u_2(x_1, x_2) = -cos(x_1)sin(x_2)F(t) \tag{7}$$

with the function $F(t) = exp\left(-2\frac{\mu}{\rho}t\right)$. To evaluate the deviation of the numerical solution in comparison with the analytical solution, the L_2 norm was used, aiding in the observation of the order of accuracy of the numerical approximation when increasing the mesh refinement – the error estimated by the norm decays quadratically with the mesh, which is equal to 10^{-5} for a 100x100 elements mesh.

The code validation was performed for Pr=0.7 and Rayleigh numbers ranging from 10^3 to 10^6. The results for the average Nusselt number were compared with the results of Davis (1983), Barakos and Mitsoulis (1994), Fusegi *et al.* (1991), and Khanafer *et al.* (2003), as shown in Table 3. The results obtained with the finite volume method presented in Section 4.1showed good agreement with the reference values.

3.2 The finite element approximation

This section presents a multi-field Galerkin least-squares formulation to approximate the mechanical model previously defined by Eq. 1, where the mass, momentum, and energy balance equations are coupled with a constitutive equation. It is important to mention that this formulation can easily accommodate non-Newtonian fluid models when applicable. The methodology does not need to satisfy the compatibility conditions between the finite element sub-spaces for extra stress-velocity and pressure-velocity – also known as the Ladyzhenskaya–Babuška–Brezzi condition. It improves the stability of the classical Galerkin method adding mesh-dependent terms – functions of the residuals of the problem governing equations – evaluated on each element. Because these residuals are trivially satisfied by the exact solution of the problem, the consistency is preserved in this class of methods.

Subjecting the system to the appropriate velocity, stress, and temperature boundary conditions, it becomes

$$\begin{aligned}
&\rho(\nabla\mathbf{u})\mathbf{u} = -\nabla p + \text{div}\ \boldsymbol{\tau} + \rho\mathbf{g}\beta(T - T_{ref}) && \text{in } \Omega \\
&\boldsymbol{\tau} = 2\mu\mathbf{D}(\mathbf{u}) && \text{in } \Omega \\
&\text{div}\ \mathbf{u} = 0 && \text{in } \Omega \\
&\rho c_p(\nabla T)\mathbf{u} = \kappa\nabla^2 T && \text{in } \Omega \\
&\mathbf{u} = \mathbf{u}_g && \text{over } \Gamma_g^{\mathbf{u}} \\
&\boldsymbol{\tau} = \boldsymbol{\tau}_g && \text{over } \Gamma_g^{\boldsymbol{\tau}} \\
&T = T_g && \text{over } \Gamma_g^{T} \\
&(-p\mathbf{I} + \boldsymbol{\tau})\mathbf{n} = \mathbf{t}_h && \text{over } \Gamma_h,
\end{aligned} \tag{8}$$

where $\boldsymbol{\tau}$ is the extra-stress tensor, $\mathbf{t}_h$ is the stress vector, and $\mathbf{u}_g$, $\boldsymbol{\tau}_g$, and T_g are, respectively, the imposed velocity, extra-stress, and temperature boundary conditions. The other variables have the same definitions as presented in Section 2.

The Galerkin least-squares approximation for the boundary value problem defined by Eq. (8) can be written as follows: given the Dirichlet and Neumman boundary conditions, find the set $\boldsymbol{\tau}^h, \mathbf{u}^h, p^h, T^h \in \boldsymbol{\Sigma}^h \times \mathbf{V}^h \times P^h \times \Theta^h$ such that

$$B(\boldsymbol{\tau}^h, \mathbf{u}^h, p^h, T^h; \mathbf{S}^h, \mathbf{v}^h, q^h, \psi^h) = F(\mathbf{S}^h, \mathbf{v}^h, q^h, \psi^h) \forall (\mathbf{S}^h, \mathbf{v}^h, q^h, \psi^h) \in \boldsymbol{\Sigma}^h \times \mathbf{V}^h \times P^h \times \Theta^h \tag{9}$$

with

$$
\begin{aligned}
B(\boldsymbol{\tau}^h, \mathbf{u}^h, p^h, T^h; \mathbf{S}^h, \mathbf{v}^h, q^h, \psi^h) &= \int_\Omega \rho(\nabla \mathbf{u}^h)\mathbf{u}^h \cdot \mathbf{v}^h d\Omega - \int_\Omega p^h \mathrm{div}\mathbf{v}^h d\Omega \; + \int_\Omega \boldsymbol{\tau}^h \cdot \mathbf{D}(\mathbf{v}^h) d\Omega \\
&+ \int_\Omega \mathrm{div}\; \mathbf{u}^h q^h d\Omega + \epsilon \int_\Omega p^h q^h d\Omega \; + \int_\Omega \boldsymbol{\tau}^h \cdot \mathbf{S}^h d\Omega \; - 2\mu \int_\Omega \mathbf{D}(\mathbf{u}^h) \cdot \mathbf{S}^h d\Omega \\
&+ \int_\Omega \rho c_p (\nabla T^h)\mathbf{u}^h \; \psi^h d\Omega \; + \int_\Omega \kappa \nabla T^h \cdot \nabla \psi^h d\Omega + \sum_{K \in \Omega^h} \int_\Omega \delta_{GLS}(\mathrm{Re}_K)\; \mathrm{div}\; \mathbf{v}^h \; \mathrm{div}\; \mathbf{u}^h d\Omega \\
&+ \sum_{K \in \Omega^h} \int_{\Omega_K} \alpha_{GLS}(\mathrm{Re}_K) \left(\rho(\nabla \mathbf{u}^h)\mathbf{u}^h + \nabla p^h - \mathrm{div}\; \boldsymbol{\tau}^h\right) \cdot \left(\rho(\nabla \mathbf{v}^h)\mathbf{u}^h \; + \nabla q^h \; - \mathrm{div}\; \mathbf{S}^h\right) d\Omega \\
&+ \beta_{GLS} \int_\Omega \left(\boldsymbol{\tau}^h \; - 2\mu \mathbf{D}(\mathbf{u}^h)\right) \cdot \left(\mathbf{S}^h \; - 2\mu \mathbf{D}(\mathbf{v}^h)\right) d\Omega \\
&+ \sum_{K \in \Omega^h} \int_{\Omega_K} \zeta_{GLS}(\mathrm{Pe}_K) \left(\rho c_p (\nabla T^h)\mathbf{u}^h - \kappa \nabla^2 T^h\right) \cdot \left(\rho c_p (\nabla \psi^h)\mathbf{v}^h - \kappa \nabla^2 \psi^h\right) d\Omega
\end{aligned}
\tag{10}
$$

and

$$
\begin{aligned}
F(\mathbf{S}^h, \mathbf{v}^h, q^h, \psi^h) &= \int_\Omega \rho\beta(T^h - T_{ref})\mathbf{g} \cdot \mathbf{v}^h d\Omega + \int_\Omega q''' \psi^h d\Omega \; + \int_{\Gamma_h} \mathbf{t}_h \cdot \mathbf{v}^h d\Gamma \\
&+ \sum_{K \in \Omega^h} \int_{\Omega_K} \alpha_{GLS}(\mathrm{Re}_K)\rho\beta(T^h - T_{ref})\mathbf{g} \cdot \left(\rho(\nabla \mathbf{v}^h)\mathbf{u}^h \; + \nabla q^h \; - \mathrm{div}\; \mathbf{S}^h\right) d\Omega \\
&+ \sum_{K \in \Omega^h} \int_{\Omega_K} \zeta_{GLS}(\mathrm{Pe}_K) q''' \left(\rho c_p (\nabla \psi^h)\mathbf{v}^h - \kappa \nabla^2 \psi^h\right) d\Omega,
\end{aligned}
\tag{11}
$$

where $\epsilon << 1$. β_{GLS} is a positive arbitrary numerical constant set according to the error estimate introduced in Behr *et al.* (1993) – in this work it was used the value 0.5. The mesh Reynolds and Péclet numbers (Re_K and Pe_K, respectively) and the stability parameters $\alpha(\mathrm{Re}_K)$, $\delta(\mathrm{Re}_K)$, and $\zeta(\mathrm{Pe}_K)$ are defined as in Behr *et al.* (1993) and references therein,

$$
\begin{aligned}
&\alpha_{GLS}(\mathrm{Re}_K) = \frac{h_K}{2\left|\mathbf{u}^h\right|_p} \xi_1(\mathrm{Re}_K) \;\; , \quad \delta_{GLS}(\mathrm{Re}_K) = \lambda_d \left|\mathbf{u}^h\right|_p h_K \xi_1(\mathrm{Re}_K) \;\; , \quad \zeta_{GLS}(\mathrm{Pe}_K) = \frac{h_K}{2\left|\mathbf{u}^h\right|_p} \xi_2(\mathrm{Pe}_K) \\
&\mathrm{Re}_K = \frac{\rho\, h_K \left|\mathbf{u}^h\right|_p m_k}{4\,\mu} \quad , \quad \xi_1(\mathrm{Re}_K) = \begin{cases} \mathrm{Re}_K, & \text{if } 0 \le \mathrm{Re}_K < 1 \\ 1, & \text{if } \mathrm{Re}_K \ge 1 \end{cases} \\
&\mathrm{Pe}_K = \frac{h_K \left|\mathbf{u}^h\right|_p m_k}{2\,\kappa} \quad , \quad \xi_2(\mathrm{Pe}_K) = \begin{cases} \mathrm{Pe}_K, & \text{if } 0 \le \mathrm{Pe}_K < 1 \\ 1, & \text{if } \mathrm{Pe}_K \ge 1 \end{cases} \\
&\left|\mathbf{u}^h\right|_p = \begin{cases} \left(\sum_{i=1}^N \left|\mathbf{u}^h\right|^p\right)^{1/p}, & \text{if } 1 \le p < \infty \\ \max_{i=1,N} \left|u_i^h\right| \quad , & \text{if } p = \infty \end{cases} \\
&m_k = \min\{1/3, 2C_k\} \;\; , \quad C_k \sum_{K \in \Omega^h} h_K^2 \left\|\mathrm{div}\; \mathbf{S}^h\right\|_{0,K}^2 \ge \left\|\mathbf{S}^h\right\|_K^2 \;\; \forall \;\; \mathbf{S}^h \in \boldsymbol{\Sigma}^h,
\end{aligned}
\tag{12}
$$

where λ_d is a positive parameter and h_K is the mesh element size. The solution strategy to solve the residual matrix problem associated with the GLS formulation was to start by obtaining a converged solution for a case of easier convergence and then to progressively use this solution as an initial estimate for the simulation pertaining to a slightly more problematic combination of parameters. The convergence criterion was to only accept solutions whose residual of the GLS-type equation was below 10^{-7} – see Zinani (2006) for further details.

3.3 Dimensionless parameters

In order to analyze the effects of the fluid properties on the heat transfer inside the cavity, the dimensionless parameters that govern the problem are obtained with the introduction of the following set of dimensionless quantities:

$$
\mathbf{x}^* = \frac{\mathbf{x}}{L_c} \; ; \quad \mathbf{u}^* = \frac{\mathbf{u}\rho L_c}{\mu} \; ; \quad \theta^* = \frac{T - T_L}{T_H - T_L} = \frac{T - T_L}{\Delta T} \; ; \quad p^* = \frac{p\rho L_c^2}{\mu^2} \; ; \quad t^* = \frac{t\mu}{\rho L_c^2} \; , \tag{13}
$$

where the dimensionless variables are indicated by the superscript *; L_c is a characteristic length, ρ and μ are taken as the properties of the simulated fluid (Tab. 1); T_H and T_L are, respectively, the temperatures of the heated and cooled walls.

Other important dimensionless paramaters in the study of convection heat transfer are the Rayleigh, Prandtl, and Nusselt numbers, defined respectively as

$$Ra = \frac{g\,\beta\,\Delta T\,L_c^3\,\rho^2\,c_p}{\mu\,\kappa}\ ,\ \ Pr = \frac{\mu\,c_p}{\kappa}\ ,\ \ Nu = \frac{h\,L}{\kappa}, \tag{14}$$

where the convection heat transfer coefficient, h, is given as the ratio between the higher temperature wall heat transfer and the temperature difference. Thus, one can rewrite Nu as

$$Nu = \frac{q''}{\Delta T}\frac{L}{\kappa} = \left(-\kappa\frac{\partial T}{\partial x_1}\right)\frac{L}{\Delta T\kappa} = -\frac{\partial\theta^*}{\partial x_1^*} \tag{15}$$

To evaluate the average Nusselt number, the local Nusselt number defined by Eq. 15 must be integrated over the whole wall length, as indicated by Eq. 16. This integral is assessed by a numerical integration method.

$$Nu_L = \int_0^L Nu(x_2)dx_2 \tag{16}$$

Table 1. Physical Properties

Properties	Base fluid	Nanoparticle	Water–copper nanofluid		
	Water	Copper	0.1%	0.5%	1.0%
κ [W/m·K]	0.604	401	0.61	0.633	0.663
c_p [J/kg·K]	4179.0	383.0	4145.2	4015.1	3863.3
ρ [kg/m^3]	997.1	8954.0	1005.1	1036.9	1076.7
μ [$\times 10^{-3}$ Pa·s]	1.0	—	1.0025	1.0127	1.0257

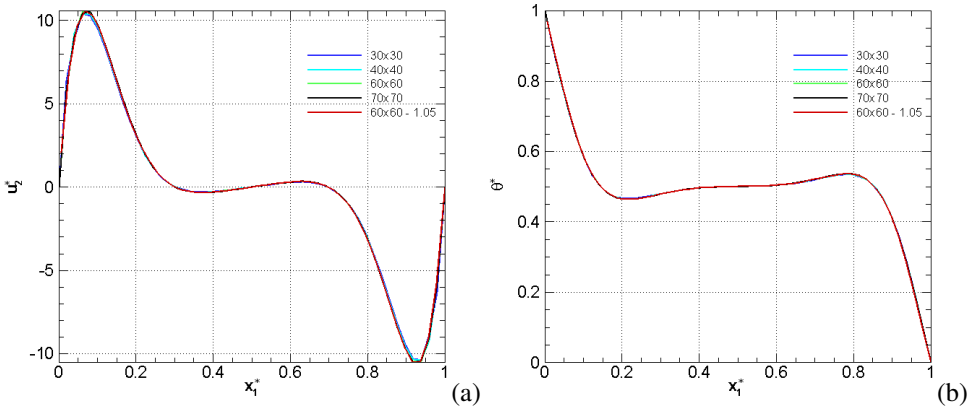

Figure 2. Results obtained at x_2^* = 0.5 with different mesh refinements for Ra = 10^5. (a) u_2^* velocity profile, (b) θ^* profile.

4. NUMERICAL RESULTS

This section presents and discusses some of the results obtained with the two above-described formulations. The effect of the volume concentration and the Rayleigh number will be analyzed in this text – these parameters control the intensity of the heat transfer inside the geometry.

4.1 Results with the Finite Volume Method

This section presents the numerical results obtained with the finite volume method for the water and water–copper nanofluid flows inside the enclosure described in Section 2. The volume concentration of copper nanoparticles ranged from 0.1% to 1.0%, whereas the Rayleigh number ranged from 10^3 to 10^5. To select the mesh to perform the numerical simulations with the finite volume method, a mesh independence test was performed based on the error on the average Nusselt number over the heated wall between consecutive refinements. Figure 2 shows the vertical velocity (u_2) and temperature profiles obtained with five different discretizations for a water flow with Ra = 10^5 – from 20×20 to 70×70 with uniform refinement and 60×60 with non-uniform refinement. One may notice the good agreement between the

results. For the simulations, the mesh with 60×60 volumes and a refinement growth rate of 5% in the length and width of the volumes from the walls toward the center of the cavity – with an error on the average Nusselt number less than 0.2% in comparison with the 70×70 mesh – was selected. This refinement was employed in order to more accurately capture the high gradients that occur near the walls.

Figure 3 shows the streamlines and temperature isolines for water flows across the range of Rayleigh numbers. One may see that at Ra = 10^3, the temperature isolines are very smooth and the streamlines indicate the existence of recirculation at the central region of the cavity. Increasing the Rayleigh number, the temperature gradients near the side walls increase. At Ra = 10^5, the central recirculation splits into two and the temperature gradients increase even more – as is shown by the proximity of the isolines (Fig. 3f) – indicating a greater heat transfer.

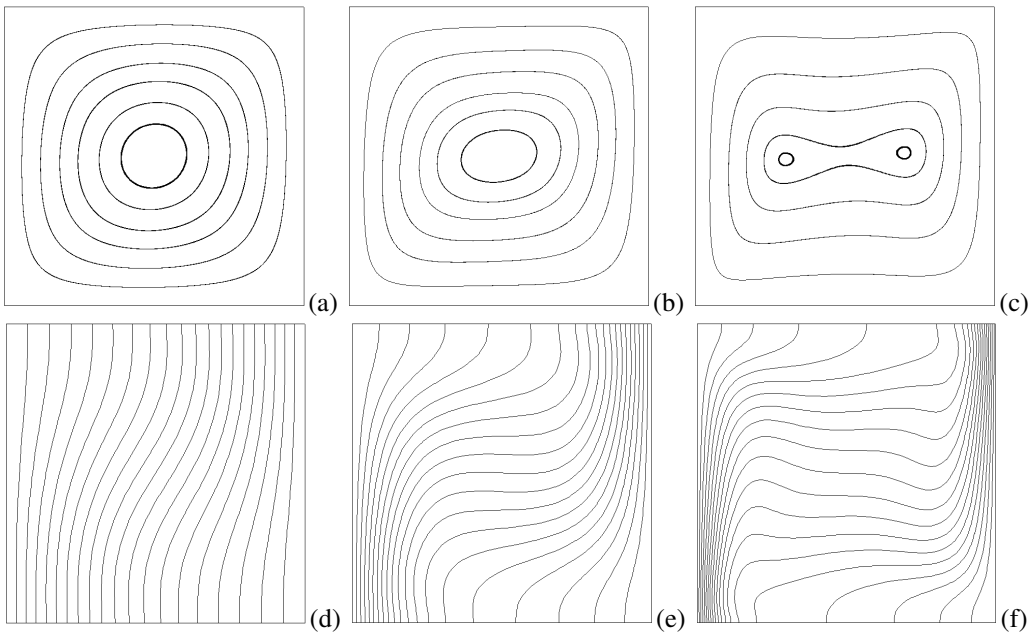

Figure 3. The flow streamlines and temperature isolines for water flow, respectively, for (a) and (d) Ra = 10^3, (b) and (e) Ra = 10^4, and (c) and (f) Ra = 10^5.

The heat transfer intensification when using nanofluids in comparison to the base fluid is shown in Fig. 4a and b, where the heat transfer coefficient profile is evaluated at the cavity heated wall – which could also have been carried out at the cooler wall. Although there is no noticeable difference between the Nusselt profile for the same Rayleigh number, as shown in Fig. 4c for 10^5, one may observe that the increase in h is directly proportional to the increase in volume concentration. This is related to the gain in thermal conductivity with the addition of nanoparticles to the base fluid (see Table 1).

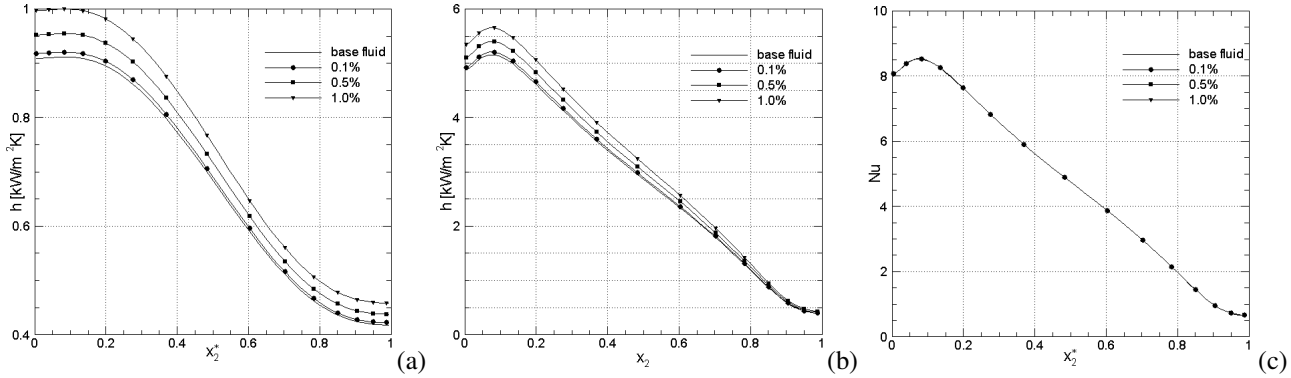

Figure 4. Heat transfer coefficient at the heated wall for (a) Ra = 10^3, (b) Ra = 10^5 and, (c) Nusselt profile at the heated wall for Ra = 10^5.

4.2 Results with the Finite Element Method

To perform the numerical simulations employing the multi-field Galerkin least-squares methodology defined by Eq. 8–12 in Section 3.2, the same mesh independence procedure based on the average Nusselt number used in Section 4. lwas

conducted. A mesh with 2500 bilinear Lagrangian (Q1) finite elements, totaling 2601 nodal points and 18,207 degrees-of-freedom, was selected. Among the meshes used, it presented the lower error in comparison with the more refined mesh, with 70×70 elements (see Table 2). The non-dimensional mesh element size, $h_K^* = h_K/L_c$, is equal to 2.83×10^{-2}.

Table 2. The average Nusselt error in comparison with the more refined mesh (70×70 elements).

Mesh	10×10	20×20	30×30	40×40	50×50
Error	4.774%	0.444%	0.102%	0.030%	0.008%

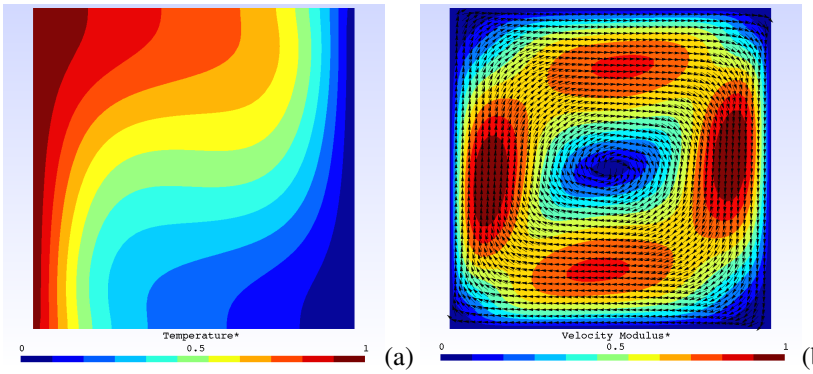

(a) (b)

Figure 5. Results for water flow, with $\mathrm{Ra} = 10^4$: (a) temperature isobands, and (b) the magnitude of the velocity vector.

It is important to observe the good stability features of the numerical approximation, as is shown by the smooth temperature isobands and the magnitude of the velocity vector obtained for $\mathrm{Ra} = 10^4$ in Fig. 5a and b, respectively. In order to validate this new methodology, Fig. 6a and b present, respectively, the temperature and vertical velocity profiles obtained with the finite volume and finite element methods. The comparison shows good agreement between the two methodologies – it is noteworthy that the finite volume formulation is validated through literature results (Table 3). The heat transfer coefficient and the Nusselt profile, presented in Fig. 6c, also show that the presented finite element methodology can provide accurate results.

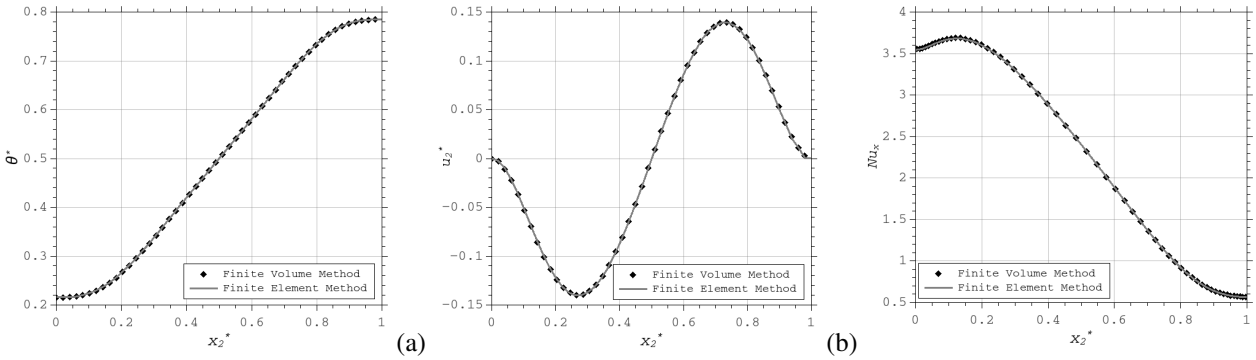

(a) (b) (c)

Figure 6. Comparison between the two employed numerical methods for at $x_1^* = 0.5$, with $\mathrm{Ra} = 10^4$: (a) temperature profile, (b) vertical velocity and, (c) Nu_x number.

Table 3. Average Nusselt comparison

Authors	Average Nusselt			
	Ra = 10^3	Ra = 10^4	Ra = 10^5	Ra = 10^6
Davis (1983)	1.118	2.243	4.520	8.799
Barakos and Mitsoulis (1994)	1.114	2.245	4.510	8.806
Fusegi *et al.* (1991)	1.105	2.230	4.646	9.012
Khanafer *et al.* (2003)	1.118	2.245	4.522	8.826
Present Work (FVM)	1.118	2.248	4.545	8.983

5. FINAL REMARKS

This work presents results obtained by two different numerical approximations of natural convection flow in a closed cavity. The thermal behavior of water and water–copper nanofluids was investigated for different Rayleigh numbers and volume concentrations of copper nanoparticles. The comparison performed showed good agreement with the literature. As expected, the increase of the Rayleigh number increased the heat transfer inside the cavity. This enhancement was more pronounced at Ra = 10^5, where the main flow recirculation at the center of the cavity splits into two – thus increasing the influence of the convective terms and increasing the heat transfer coefficient. The nanoparticle volume concentration plays an important role in the increase of the heat transfer coefficient, which is associated with the increase in the thermal conductivity. It is important to mention the stability of the finite element formulation presented in this work providing satisfactory results even for a very coarse mesh – as shown in Table 2. The presented results give encouraging perspectives for application to non-Newtonian fluids and complex geometries.

6. ACKNOWLEDGEMENTS

The authors acknowledge FAPEMIG and the Faculty of Mechanical Engineering (FEMEC/UFU) for financial support.

7. REFERENCES

Abu-Nada, E., Masoud, Z., Oztop, H.F. and Campo, A., 2010. "Effect of nanofluid variable properties on natural convection in enclosures". *International Journal of Thermal Sciences*, Vol. 49(3), pp. 479–491. doi: 10.1016/j.ijthermalsci.2009.09.002.

Aminossadati, S.M. and Ghasemi, B., 2009. "Natural convection cooling of a localised heat source at the bottom of a nanofluid-filled enclosure". *European Journal of Mechanics – B/Fluids*, Vol. 28(5), pp. 630–640. doi: 10.1016/j.euromechflu.2009.05.006.

Barakos, G. and Mitsoulis, E., 1994. "Natural convection flow in a square cavity revisited: laminar and turbulent models with wall functions". *International Journal of Numerical Methods for Heat and Fluid Flow*, Vol. 18, pp. 695–719.

Batchelor, G.K., 1977. "The effect of brownian motion on the bulk stress in a suspension of spherical paricles". *Journal of Fluid Mechanics*, Vol. 83, pp. 97–117.

Behr, A.M., Franca, L.P. and Tezduyar, T.E., 1993. "Stabilized finite element methods for the velocity – pressure – stress formulation of incompressible flows". *Computer Methods in Applied Mechanics and Engineering*, Vol. 104, pp. 31–48.

Choi, S.U.S. and Eastman, J.A., 1995. "Enhancing thermal conductivity of fluids with nanoparticles". *Developments and Applications of Non-Newtonian Flows*, Vol. 66, pp. 99–105.

Davis, G.V., 1983. "Natural convection of air in a square cavity: a bench mark numerical solution". *International Journal for Numerical Methods*, Vol. 3, pp. 227–248.

Fusegi, T., Hyun, J.M., Kuwahara, K. and Farouk, B., 1991. "A numerical study of three-dimensional natural convection in a differentially heated cubical enclosure". *International Journal of Heat and Mass Transfer*, Vol. 34, pp. 1543–1557.

Khanafer, K., Vafai, K. and Lightstone, M., 2003. "Buoyancy-driven heat transfer enhancement in a two-dimensional enclosure utilizing nanofluids". *International Journal of Heat and Mass Transfer*, Vol. 46, pp. 3639–3653. doi: 10.1016/S0017-9310(03)00156-X.

Masuda, H., Ebata, A., Teramae, K. and Hishinuma, N., 1993. "Alteration of thermal conductivity and viscosity of liquid by dispersing ultra-fine particles". *Netsu Bussei*, Vol. 4, pp. 227–233.

Maxwell, J.C., 1873. *A treatise on electricity and magnetism*. Clarendon Press, Oxford.

Putra, N., Roetzel, W. and Das, S., 2003. "Natural convection of nano-fluids". *Heat and Mass Transfer*, Vol. 39(8-9), pp. 775–784. doi:10.1007/s00231-002-0382-z.

Taylor, G.I. and Green, A.E., 1937. "Mechanism of the production of small eddies from large ontes". *Proceedings of the Royal Society of London. Series A, Mathematical and Physical Sciences*, Vol. 158, pp. 499–521.

Wang, B., Zhou, L. and Peng, X., 2003. "A fractal model for predicting the effective thermal conductivity of liquid with suspension of nanoparticles". *International Journal of Heat and Mass Transfer*, Vol. 46, pp. 2665–2672.

Wang, X., Mujumdar, A. and Yap, C., 2006. "Free convection heat transfer in horizontal and vertical rectangular cavities filled with nanofluids". In *International Heat Transfer Conference*. doi:10.1615/IHTC13.p6.410.

Zinani, F.S.F., 2006. *Desenvolvimento e implementação computacional de formulações Galerkin mínimos-quadrados para escoamentos não Newtonianos sensíveis à cinemática*. Ph.D. thesis, Universidade Federal do Rio Grande do Sul.

8. RESPONSIBILITY NOTICE

The authors are the only responsible for the printed material included in this paper.